HHS Public Access

Author manuscript

Neurobiol Dis. Author manuscript; available in PMC 2025 May 12.

Published in final edited form as:

Neurobiol Dis. 2025 May ; 208: 106879. doi:10.1016/j.nbd.2025.106879.

Dicer deficiency affects microglial function during demyelination and impairs remyelination

Ajai Tripathi[a,1], **Nagendra Kumar Rai**[a,1], **Aaron Perles**[a], **Haley Courtney**[a], **Claire Jones**[a], **Adya Sapra**[a], **Jason Plemel**[b], **Ranjan Dutta**[a,c,*]

[a]Department of Neurosciences, Cleveland Clinic, Cleveland, OH, USA

[b]Neuroscience and Mental Health Institute, Department of Medicine, Division of Neurology, Department of Medical Microbiology and Immunology, University of Alberta, Canada

[c]Cleveland Clinic Lerner College of Medicine, Cleveland, OH, USA

Abstract

Microglia are essential regulators of central nervous system (CNS) homeostasis, playing key roles in demyelination and remyelination. Dysregulated microglial activity contributes to pathological inflammation and impaired repair processes in demyelinating diseases. Here, we investigate the role of *Dicer1*, a critical enzyme in microRNA biogenesis, in affecting microglial function, demyelination, and remyelination. Loss of *Dicer1* in microglia resulted in amplified inflammatory responses, defective myelin debris clearance, and disruption of metabolic homeostasis, leading to exacerbated demyelination and delayed remyelination. Transcriptomic analysis revealed significant upregulation of inflammatory pathways, including interferon signaling and *JAK/STAT* activation, alongside a loss of homeostatic microglial gene expression. Protein-level validation confirmed sustained secretion of pro-inflammatory cytokines such as *IFN-γ, IL-16*, and *CXCL12*, creating a chronic inflammatory environment that impaired remyelination. Furthermore, *Dicer1*-deficient microglia failed to support oligodendrocyte progenitor cells (OPCs) differentiation/maturation, with increased apoptosis of mature oligodendrocytes (OLs),

*Corresponding author at: Department of Neurosciences, Lerner Research Institute, Cleveland Clinic, 9500 Euclid Avenue/NC30, Cleveland, OH 44195, USA., duttar@ccf.org (R. Dutta).

[1]These authors have contributed equally.

Supplementary data to this article can be found online at https://doi.org/10.1016/j.nbd.2025.106879.

Lead contact

Further information will be addressed by the Lead Contact, Ranjan Dutta (duttar@ccf.org). RNA sequencing data files have been deposited at Gene Expression Omnibus (GEO) with accession number GSE263765.

CRediT authorship contribution statement

Ajai Tripathi: Writing – review & editing, Writing – original draft, Validation, Methodology, Investigation, Formal analysis, Conceptualization. **Nagendra Kumar Rai:** Writing – review & editing, Writing – original draft, Visualization, Formal analysis, Conceptualization. **Aaron Perles:** Validation, Data curation. **Haley Courtney:** Formal analysis, Data curation. **Claire Jones:** Methodology, Formal analysis. **Adya Sapra:** Methodology, Formal analysis. **Jason Plemel:** Visualization, Formal analysis. **Ranjan Dutta:** Writing – review & editing, Writing – original draft, Validation, Supervision, Resources, Project administration, Methodology, Funding acquisition, Formal analysis, Data curation, Conceptualization.

Declaration of competing interest

The authors declare the following financial interests/personal relationships which may be considered as potential competing interests: Ranjan Dutta reports financial support was provided by National Institute of Neurological Disorders and Stroke. If there are other authors, they declare that they have no known competing financial interests or personal relationships that could have appeared to influence the work reported in this paper.

contributing to remyelination failure. These findings identify Dicer1 as a critical regulator of microglial homeostasis and inflammation resolution, highlighting its potential as a therapeutic target to mitigate inflammation and promote repair in demyelinating diseases.

Keywords

Microglia; *Dicer1* ; microRNA; Cytokines; Inflammation; Demyelination; Remyelination

1. Introduction

Microglia, the tissue-resident macrophages of the central nervous system (CNS), arise from myeloid progenitor cells in the embryonic yolk sac. These innate immune cells play critical roles in normal brain development and homeostasis, including maintaining oligodendrocyte progenitor cells (OPCs) number and supporting oligodendrocytes (OLs) maturation and myelination (Djannatian et al., 2023; Nemes-Baran et al., 2020; Wlodarczyk et al., 2017). Recent studies have reported dysregulated microglial activities in various neurodegenerative diseases including multiple sclerosis (MS), a chronic inflammatory demyelinating disease of the CNS. In MS, OL damage, myelin destruction, and accompanying neuronal loss have been associated with activated microglia/macrophages in and around demyelinating lesions (Plemel et al., 2020). Nonetheless, microglia also repopulate remyelinating lesions and promote remyelination through the expression of anti-inflammatory molecules, phagocytosis of myelin debris, and repair of tissues (Cignarella et al., 2020; Lampron et al., 2015a; Lloyd et al., 2019; Miron et al., 2013). Thus, identifying mechanisms regulating the pathogenic and protective functions of microglia is critical for designing targeted therapeutic interventions for MS.

Emerging evidence suggests that epigenetic modulators (microRNAs (miRNAs) and histone modifications) regulate cellular behavior in both physiological and pathological conditions (Hwang et al., 2017). miRNAs, which are short non-coding RNAs, are processed to mature form by a ribonuclease type III, Dicer (DICER) enzyme, and regulate post-transcriptional gene expression by binding to the 3’UTR region of target genes. Various studies have identified critical direct and indirect roles for *Dicer1*-regulated miRNAs expression in normal glial cell functions and development, including OL differentiation and maturation as well as axonal myelination/remyelination (Dugas et al., 2010; Shin et al., 2009; Tripathi et al., 2019; Zhao et al., 2010). For example, astrocyte involvement in OL differentiation and myelination/remyelination has been found to be affected by miRNAs regulating target gene expression (Liu et al., 2021). A recent study has also examined the importance of adult microglial miRNAs and reported that miRNAs are required for microglial responses to inflammatory challenges (Varol et al., 2017). The current study focused on the effects of microglial miRNAs in the process of demyelination and remyelination.

In this study, we investigated the consequence of microglia-specific *Dicer1* loss on the processes of demyelination and remyelination. We found that Dicer positive microglia number declined in the center of white matter lesion (WML) of MS brain tissue. We used TMX inducible microglial ($Cx3cr1^{creERT2}$) and CNS resident microglia specific

(Tmem119^{creERT2}) *Dicer1*-ablated mouse lines to demonstrate the importance of microglial miRNA expression in demyelinating/remyelinating conditions. Loss of microglial *Dicer1* expression led to a significant decline in microglia/macrophage number, without affecting CNS myelination in the corpus callosum region (CC, equivalent to the white matter region of the human brain) of mouse brain. Additionally, *Dicer1*-deficient microglial cells assumed a hyperactive phenotype and caused extensive myelin loss following cuprizone-induced demyelination. Transcriptomic analyses revealed a significant upregulation of inflammatory pathways, including *JAK/STAT* and interferon signaling, alongside a suppression of homeostatic microglial genes. Furthermore, *Dicer1*-deficient microglia exhibited sustained secretion of proinflammatory cytokines, creating a chronic inflammatory environment that impaired OPC differentiation and promoted apoptosis of mature OLs, ultimately delaying remyelination. These findings demonstrate the critical role of *Dicer1* in regulating microglial activation and affecting the process of repair in demyelinating diseases.

2. Materials and methods

Detailed information about all resources used in the study has been shown in Supplementary Table 1.

2.1. Human subjects

Human brains were collected as part of the tissue procurement program approved by the Cleveland Clinic Institutional Review Board. The MS patient's postmortem brain tissue (Supplementary Table 2) was collected according to a rapid autopsy protocol at the Cleveland Clinic and sliced (1 cm thick) using a guided box. Slices were short-fixed in 4 % paraformaldehyde followed by cryoprotection and 30 μM thickness sectioning using sliding microtome. Serial MS brain sections were immunostained with rat anti-PLP (1:300, Gift from Dr. Wendy Macklin), mouse anti-MHCII (1:250, Novus Biologicals), mouse anti-IBA1 (1:500, Abcam), mouse anti-GFAP (1:200, BioLegend), anti-ASPA (1:250, ORIGENE), and rabbit anti-Dicer (1:250, Novus Biologicals) as previously reported (Dutta et al., 2019).

2.2. Mouse models

All procedures were approved by the Institutional Animal Care and Use Committee (IACUC) at the Lerner Research Institute (LRI), Cleveland Clinic Foundation (Cleveland, OH). Wild-type (C57BL/6 J, Stock #00664) and transgenic mice (Cx3cr1^{creERT2}, stock# 020940; Tmem119^{creERT2}, stock# 031820; and Dicer$^{fl/fl}$, stock# 06001) were procured from Jackson Laboratory and maintained on a 12 h light/dark cycle with access to food and water ad libitum. All mouse experiments were performed from CNS tissue collected from P1/P6–7 (either sex) to the adult stage (male, 4–22 weeks).

2.3. Transgenic animal models and genotyping Dicer Floxed recombined alleles

The inducible Cx3cr1^{creERT2} /Tmem119^{creERT2}xDicer$^{fl/fL}$ (iKO) mouse line was generated by breeding Cx3cr1^{creERT2} /Tmem119^{creERT2} and Dicer$^{fl//fl}$ mice and genotyped using primers targeting CRE insert and flox site (Supplementary Table 3). Littermate CRE-negative (Cx3cr1 Cre−: Dicer$^{fl/fl}$ *and* Tmem119 Cre−: Dicer$^{fl/fl}$) animals were used as controls for in vivo experiments and labeled as Cre(−) or control, whereas mutant (*Dicer1*

ablated), Cre + (Cx3cr1 Cre+: Dicer$^{fl/fl}$ *and* Tmem119 Cre+: Dicer$^{fl/fl}$), were labeled as Cre(+), mutant.

2.4. Tamoxifen (TMX) treatment

To induce recombination in transgenic mice, TMX (Sigma, # T5648, 10 mg/mL) was suspended in warm corn oil and administered intraperitoneally for five constitutive days at 75 mg/kg BW. All animals were TMX-treated at 4–5 weeks of age and observed for 3–4 weeks before starting cuprizone (CUP) feeding.

2.5. Cuprizone (bis–cyclohexanone-oxaldihydrazone)-induced demyelination

Seven- to eight-week-old male animals were maintained on 0.3 % cuprizone (CUP)-supplemented diet (ENVIGO) for 6 weeks. For naïve controls, littermate animals were maintained on normal chow. After 6 weeks, animals were euthanized, and brain samples were collected. For remyelination groups, animals were transferred to normal chow for an additional six weeks, before collecting the brain tissue.

2.6. BrdU incorporation assay

To identify proliferating glial cells during demyelination, BrdU (100 μg, Sigma) was administered intraperitoneally for six consecutive days at five weeks of cuprizone treatment (Cignarella et al., 2020). At the end of the demyelination period (2 h after the last BrdU injection), animals were euthanized and brain samples were collected for IHC analysis (Mi et al., 2016).

2.7. Immunohistochemistry

Cre−/+ animals were euthanized and transcardially perfused with 4 % paraformaldehyde (PFA). Brains were fixed in 4 % PFA (48 h) followed by equilibration in 30 % sucrose solution for 48 h. Subsequently, brains were coronally sliced with a cooled microtome into 30 μm thick sections. Sections were stained with rat anti-PLP (1:300, Gift from Dr. Wendy Macklin), rabbit anti-IBA1 (1:750, Abcam), mouse anti-APC (1:250, Millipore), goat anti-PDGFRα (1:250, R&D system), rabbit-cleaved caspase 3 (1:250, Cell signal), rat anti-CD68 (1:500, BioLegend), rat anti-BrdU (1:250, Abcam), rabbit antidegraded myelin basic protein (dMBP) as previously described (Dutta et al., 2019). Primary antibody incubations were followed by corresponding secondary antibody labelling using respective Alexa fluor-tagged donkey anti-rat/rabbit/mouse/goat (Thermo Scientific) secondary antibodies. In MS brain tissue section, PLP and MHC II-diaminobenzidine (DAB) immunohistochemistry was performed using biotinylated secondary Abs (Vector Laboratories) following primary Ab incubation, overnight at 4 °C; biotin–avidin–peroxidase complex (Vector Laboratories) and DAB (Vector Laboratories) were used as the developing agent (Dutta et al., 2019). For Oil Red O (ORO) staining (Mehlem et al., 2013), frozen sections were fixed in 60 % isopropyl alcohol for 30 s, stained with ORO solution for 10 min, and washed to remove excess dye. After rinsing with PBS, sections were mounted in glycerin, and images were captured using a Leica DM5500B light microscope.

2.8. BV2 cell cultures and primary microglia cultures

BV2 cells (kindly provided by Dr. Feng Ling, Cleveland Clinic) were cultured in Dulbecco's modified Eagle's medium (DMEM) high glucose containing 5 % fetal bovine serum (FBS), 100 IU/mL penicillin (pen), and 100 mg/mL streptomycin (strep) and incubated at 37 °C and 5 % CO_2. Mouse brain primary microglia were isolated from P1 pups of either sex by mixed glia culture methods. Briefly, pup brains were dissected and cut into small 1 mm^3 pieces before digesting in HBSS containing 200 U papain and 2500 U DNAseI at 37 °C for 30 min. The cell suspension was filtered through a 40 μm-strainer and resuspended in growth media (DMEM+10 %FBS + 1× Pen-strep). The mixed glia cells were maintained in growth media at 37 °C and 5 % CO_2 with media changes every other day until day 10–12. To collect loosely attached microglia cells, flasks were shaken at 150 rpm, 37 °C and 5 % CO_2 for 1 h before transferring media with detached microglia cells to 12-mm poly-D-lysine-coated coverslips in a new 24-well tissue culture plate.

2.9. Primary microglia siRNA transfection

Primary microglia were transfected by *Dicer1* siRNA (Dharmacon siRNAs SMARTpool) and Lipofectamine RNAiMAX Transfection Reagent following manufacturer's instructions using a siRNA to Lipofectamine ratio of 1:2. Before microglia transfection, fresh growth media was added to cells and transfected with 5 pmol siRNAs per well of a 24-well plate. Scrambled siRNA was used as an experimental control.

2.10. Lenti-Dicer1 Crispr/Cas9 generation

Mouse *Dicer1* guide RNA (gRNA), AACCGTACACTGTCCATCGG, was designed using the ChopChop online guide RNA design tool and cloned in Lenti-CRISPR-Cas9 plasmid (lentiCRISPR v2 was a gift from Feng Zhang, Addgene plasmid # 52961; http://n2t.net/addgene:52961; RRID:Addgene_52,961) as previously reported (Sanjana et al., 2014). To generate lentivirus expressing *Dicer1* gRNA, cloned lentiCRISPR plasmid and 2nd generation packaging system (psPAX2 and pCMV-VSV-G) were co-transfected to HEK cells using Lipofectamine 3000 transfection reagent (Thermo Fisher) as per the manufacturer's protocol (psPAX2 was a gift from Didier Trono (Addgene plasmid # 12260; http://n2t.net/addgene:12260; RRID: Addgene_12,260, pCMV-VSV-G was a gift from Bob Weinberg (Addgene plasmid # 8454; http://n2t.net/addgene:8454; RRID: Addgene_8454). After 24 h post-transfection (day 0), fresh growth media (DMEM GlutaMax+10 % FBS + 1× antibiotics) was added and lentivirus particles containing media were collected over the following two days (day 1 and day 2) and further concentrated using an ultracentrifugation method as previously reported (Tripathi et al., 2019).

2.11. Stable BV2 Dicer knockout cell line

To create the *Dicer1* knockout cell line, BV2 cells were transduced with lentivirus expressing *Dicer1* gRNA-Cas9 using polybrene (10 μg/mL, Sigma) transfection reagent as previously described (Tripathi et al., 2019). Transduced BV2 cells were further selected with puromycin antibiotic (4 μg/mL) to create a stable cell line. For controls, lentiCripsrV2-Cas9 empty vector expressing lentivirus was used.

2.12. Myelin phagocytosis

For the phagocytosis experiment, myelin was isolated from the adult mouse brain using a Percoll density gradient method (Yip et al., 2019). To analyze myelin uptake by *Dicer1* KO BV2 cells, myelin (10 μg/mL) was added to the culture medium. After 24 h incubation, cells were washed, lysed, and protein was isolated for western blot analysis.

2.13. Mouse brain primary OPC cultures

Mouse brain primary OPCs were isolated from P6-P7 mouse pups of either sex by an immunopanning method as previously described (Tripathi et al., 2019). Briefly, CD140a-positive cells were serially immunopanned to enrich OPCs and cultured in serum-free OPC proliferation medium (DMEM, glutamine- 2 mM, sodium pyruvate- 1 mM, insulin- 5 μg/mL, *n*-acetyl-cysteine- 5 μg/mL, trace element B- 1×, d-biotin- 10 ng/mL, B27– 1×, antibiotic-antimycotic- 1×, BSA-10 μg/mL, transferrin-10 μg/mL, putrescine- 1.6 μg/mL, progesterone- 60 ng/mL, selenite- 40 ng/mL, PDGFα- 20 ng/mL, NT3–2 ng/mL, forskolin- 4.2 μg/mL, CNTF- 10 ng/mL) and seeded on a microglia monolayer cultured on poly-D-lysine-coated 12-mm diameter glass coverslips in a 24-well plate (50,000 cells/coverslip). After 24 h in proliferation conditions, old media was replaced with fresh OL differentiation media (OPC media +T3 (40 ng/mL).

2.14. RNA extraction and reverse transcription-quantitative polymerase chain reaction (RT-qPCR)

Total RNA was isolated from sorted mouse CNS microglia ($CD45^{lnt}$/Cd11b + cells) and primary microglia using Qiagen RNA isolation kits (Qiagen) as per the manufacturer's instructions. Total RNA was reverse transcribed to cDNA by SuperScript™ VILO™ cDNA Synthesis Kits (Applied Biosystems) as recommended, respectively. The expression of *Dicer1* was assessed using TaqMan Gene expression assays (Thermo-Fisher). GAPDH was used as an endogenous control in the reaction. Delta Ct values were used to determine relative expression changes ($2^{-\Delta\Delta CT}$) and are presented as fold change (FC).

2.15. Western blotting

Total protein was extracted from stable BV2 cells in RIPA lysis buffer (Thermo Fisher) supplemented with 1× Halt protease and phosphatase inhibitor cocktails (Thermo Fisher). Ten micrograms (10 μg) of total protein from each sample were resolved on 4–12 % SDS-PAGE gels and transferred to PVDF membranes. Membranes were blocked in 5 % non-fat dry milk in tris-buffered saline with Tween-20 (TBST) for 1 h at room temperature followed by incubating membranes overnight at 4 °C in the following primary antibodies: rat anti-MBP (1:500) and mouse anti-GAPDH (1:5000). After washing in TBS-T, blots were then incubated with peroxidase-conjugated anti-mouse (1:10000) and anti-rat IgG (1:1000) for 1 h at RT. Chemiluminescence bands were detected with Clarity Western ECL substrate (Bio-Rad Laboratories, Hercules, CA) and imaged using a Bio-Rad Chemidoc MP and analyzed using Image Lab software (ver. 5).

2.16. Cytokine array

A mouse cytokine array kit (R&D Systems, Cat #ARY006) was utilized to simultaneously measure 40 mouse cytokines in Cx3cr1^{creERT2} Cre− and Cre + demyelination/remyelination brain samples, following the manufacturer's protocol. In brief, whole brains were collected and homogenized in freshly prepared lysis buffer (PBS containing protease inhibitors: 10 μg/mL Aprotinin, 10 μg/mL Leupeptin, 10 μg/mL Pepstatin, and 1 % Triton X-100). A total of 300 μg of tissue lysate was combined with array buffers and detection antibody cocktails and incubated overnight at 4 °C on a platform shaker with pre-coated capture antibody membranes. The signal was developed using West-Femto Maximum Sensitivity Substrate (Thermo Fisher Scientific), and images were captured with a Bio-Rad Chemidoc MP, followed by analysis with Image Lab software (version 5).

2.17. Immunofluorescence

Fixed cells (OLs/microglia) were permeabilized with 0.1 % Triton-X100 for 10 min at room temperature. After washing in PBS (3×), samples were blocked in 5 % normal goat serum (NGS) and 1 % BSA for 1 h at RT. Samples were incubated with primary antibodies (MBP- 1:300 and IBA1–1:500) overnight at 4 °C. The next day, after washing in PBS (3×), cells were incubated in Alexa fluorophore-tagged compatible secondary antibodies for 1 h at room temperature. After washing (PBS), cells were mounted in prolong gold antifade (+DAPI) mounting media.

2.18. Image acquisition, processing, and quantification

Fluorescent images were obtained with a Leica DM5500 fluorescence microscope (Leica, New Jersey, USA) and a confocal laser-scanning microscope (Zeiss, Oberkochen, Germany) at appropriate excitation wavelengths and magnification. All confocal images were acquired as stacks of ~50 slices imaged at ~25 μm depth using a 20×−40× objective. These image slices were then stacked together using FIJI (IMAGE J) software for the generation of the final image. Images were processed and quantified (cell number, area occupied) using FIJI (IMAGE J) software (Schindelin et al., 2012). For statistical analysis, a region of interest (ROI) within the corpus callosum (CC) was chosen from the acquired images and analyzed for cell counting, and further normalized to the area examined for each animal.

2.19. Microglia fluorescence-activated single cell sorting (FACS)

Brains from naïve control, demyelination (CUP-6w), and remyelination (6 + 6w) Cxcr1^{creERT2} Cre− and Cre + male mice were homogenized using a Neural Tissue Dissociation Kit (Papain, Miltenyi Auburn, CA) following the manufacturer's protocol. Cells were re-suspended in RPMI containing 25 mM HEPES (pH −7.2), adjusted to 30 % Percoll (Pharmacia, Uppsala, Sweden), underlaid with 1 mL 70 % Percoll and centrifuged at 850 ×*g* for 30 min at 4 °C. Cells were collected from the 30 %/70 % interface, washed with RPMI, counted, and suspended in FACS buffer (0.1 % Bovine serum albumin in DPBS). Fcγ receptors were blocked with 1 % mouse serum and rat anti-mouse CD16/32 mAb (clone 2.4G2: BD Biosciences, San Diego, CA) for 20 min on ice prior to staining with CD45 (clone 30-F11) and CD11b (clone M1/70) antibodies in FACS buffer. Microglia were sorted based upon their CD45^{int}CD11b + phenotypes using a FACS Aria III (BD Biosciences) and

FACS Diva software (BD Biosciences). For RNA-seq study, sorted cells were collected in 1.5 mL microfuge tubes containing RNase inhibitor before subsequent centrifugation. Cell pellets were re-suspended in Trizol (Invitrogen, Carlsbad, CA) and stored at −80 °C until RNA-seq.

2.20. RNA-seq and data analysis

RNA was isolated from FACS microglia ($CD45^{int}$/CD11b+) and quantified using a Qubit 2.0 Fluorometer (Life Technologies, Carlsbad, CA, USA). RNA integrity was assessed with 2100 TapeStation (Agilent Technologies, Palo Alto, CA, USA). SMART-Seq v4 Ultra Low Input Kit for Sequencing was used for full-length cDNA synthesis and amplification (Clontech, Mountain View, CA), and an Illumina Nextera XT library was used for sequencing library preparation. The final library was assessed with Qubit 2.0 Fluorometer and Agilent TapeStation. The samples were sequenced using a 2 × 150 Paired End (PE) configuration on the Illumina HiSeq instrument according to the manufacturer's instructions. Image analysis and base calling were conducted by the HiSeq Control Software (HCS) on the HiSeq instrument. Raw sequence data (.bcl files) generated from Illumina HiSeq were converted into fastq files and de-multiplexed using Illumina bcl2fastq v. 2.17 program. One mismatch was allowed for index sequence identification. After demultiplexing, sequence data were assessed for overall quality and yield. Then, sequence reads were trimmed to remove possible adapter sequences and nucleotides with poor quality using Trimmomatic v.0.36. The trimmed reads were mapped to the *Mus musculus* mm10 reference genome available on ENSEMBL using the STAR aligner v.2.5.2b. The STAR aligner uses a splice aligner that detects splice junctions and incorporates them to help align the entire read sequences. BAM files were generated as a result of this step. Unique gene hit counts were calculated by using featureCounts from the Subread package v.1.5.2. Only unique reads that fell within exon regions were counted. After the extraction of gene hit counts, the gene hit counts table was used for downstream differential expression analysis. Using DESeq2, a comparison of gene expression between the groups of samples was performed. The Wald test was used to generate *p*-values and Log2 fold changes. Genes with adjusted p-values <0.05 and absolute log2 fold changes > (±) 1 were considered as differentially expressed genes (DEGs) for each comparison.

2.21. Bioinformatics analysis

Gene Ontology (GO) enrichment analysis using Enrichr identified key biological processes affected by *Dicer1* deletion, with pathways filtered at an adjusted p-value <0.01 and visualized via bar plots. Pre-ranked Gene Set Enrichment Analysis (GSEA) ranked genes by log2 fold change and assessed enrichment against MSigDB Hallmark and Gene Ontology gene sets, with pathways considered significant at NES > ±1 and FDR < 0.05. Heatmaps generated using Morpheus highlighted altered pathways, including cell cycle regulation, cholesterol metabolism, and phagocytosis, illustrating transcriptional differences between *Dicer1*-deficient and control microglia.

2.22. Quantification and statistical analysis

All data analyses were performed using GraphPad Prism 8.0. Quantifications were performed from at least three or more animals for in vivo study or independent in vitro

experiments and in a blinded fashion. Statistical analysis was performed using Student's *t*-tests to compare between two groups and one-way ANOVA for 3 or more groups (Supplementary Table 4). $P < 0.05$ was considered to be statistically significant. Data are shown as mean ± standard error of the mean (SEM).

3. Results

3.1. Dicer1 Expression in MS lesions and microglial activation

Multiple focal areas of myelin loss accompanied by inflammation and gliosis within the CNS are the main pathologic hallmarks of MS (Kuhlmann et al., 2017). To characterize MS demyelinating lesions, serial brain sections were immunostained for myelin (anti-PLP) and lesion-associated immune cells (Anti-MHC II) (Fig. 1A and B). As Dicer protein levels has been found to be significantly lower in MS patients (Aung and Balashov, 2015; Magner et al., 2016), we immunostained serial brain sections from histologically characterized MS brain tissues for Dicer protein in microglia/macrophages (IBA1), astrocytes (GFAP), and oligodendrocytes (ASPA) (Fig. 1C–1H). Interestingly, the majority of Dicer expressing cells were found to be IBA1+ microglia/macrophages in normal-appearing white matter (NAWM) (Fig. 1 Ci–ii), and lesion center (LC) (Fig. 1 Di–ii) of MS lesions, whereas a minimal number of astrocytes (Fig. 1E–1F) and oligodendrocytes (Fig. 1G–1H) were found to be Dicer positive. Interestingly, there was a significant decrease in the number of Dicer expressing IBA1+ cells in MS LC compared to NAWM (Fig. 1I), indicating Dicer positive microglia/macrophages population decline during demyelination in MS brain.

3.2. Dicer1 deleted microglial response to demyelination

Loss of postnatal microglial miRNA expression led to decreased microglial numbers in mouse brain cortex and hippocampal regions (Varol et al., 2017). To test and distinguish the effects of tamoxifen (TMX) injection and loss of *Dicer1* expression postnatally in CNS resident microglia/macrophages, we used two mouse lines ($Cx3cr1^{creERT2}$ and $Tmem119^{creERT2}$) and compared microglial number in brain white matter (WM) regions (corpus callosum, CC, Supplementary Figure S1A and S1B), with the maximum demyelination susceptibility. For all studies, TMX-injected male mice from Cre + ($X^{CreERT2+/+}/Dicer^{fl/fl}$) and Cre-ve ($X^{CreERT2-/-}/Dicer^{fl/fl}$) were used (X- Cx3cr1 or Tmem119). TMX-induced Dicer1 deletion led to 62 % and 22 % decline in IBA1+ microglia/macrophage numbers within the CC of Cre + mutant animals compared to littermate Cre− controls in $Cx3cr1^{creERT2}$ and $Tmem119^{creERT2}$ cohort, respectively (Supplementary Figs. S1C vs S1D, and S1K; S1O vs S1P, and S1W). However, *Dicer1* loss in adult microglia/macrophages cells did not affect CC myelin content (Supplementary Figs. S1E vs S1F, and S1L; S1Q vs S1R, and S1X) or OLs/OPCs cell density, indicating that *Dicer1* deletion does not impair myelin maintenance under non-pathological conditions (Supplementary Figs. S1G–S1J, S1M, S1N, and S1S–S1V, S1Y and S1Z).

After peripheral endotoxin exposure, *Dicer1*-deficient microglia show heightened inflammatory responses (Varol et al., 2017). Thus, to examine microglial response during demyelination, we used $Cx3cr1^{creERT2}/Dicer1^{fl/fl}$ and $Tmem119^{creERT2}/Dicer1^{fl/fl}$ mouse lines, and induced tamoxifen-mediated Cre recombinase to ablate *Dicer1* expression,

followed by six weeks of 0.3 % cuprizone (CUP) treatment to induce demyelination (Fig. 2A and N). In both mouse lines, *Dicer1*-ablated (Cre+) mice exhibited 45 %–55 % less myelin than Cre− controls (Cx3cr1^{creERT2}- Fig. 2B vs 2C, and 2 J; Tmem119^{creERT2}- Fig. 2O vs 2P, and 2 W). As expected, myelin loss was accompanied by increased microglial activation, shown by elevated IBA1+ cell counts (Cx3cr1^{creERT2}–71 %, Fig. 2D vs 2E and 2 K; Tmem119^{creERT2}–40 %, Fig. 2Q vs 2R and 2X). Notably, Cx3cr1^{creERT2} mice showed a greater increase in IBA1-positive microglia compared to controls, which was more pronounced than Tmem119^{creERT2} mouse line (71 % vs 40 %), indicating a stronger microglial activation response to demyelination. Both mouse lines also showed decreased mature oligodendrocyte counts (APC+/OLIG2+) under demyelination conditions (Cx3cr1^{creERT2}–45 %, Figs. 2F vs 2G, and 2 L; Tmem119^{creERT2}–25 %, Figs. 2S vs 2 T, and 2Y). On the contrary, OPCs (PDGFRα+OLIG2+ cells) population showed an increase trend in Cx3cr1^{creERT2} mice (Figs. 2H vs 2I, and 2 M), and a significant increase in Tmem119^{creERT2} line (~2.1 folds, Figs. 2U vs 2 V, and 2Z) suggesting a possible compensatory response to ongoing demyelination.

3.3. Microglial Dicer1 affects oligodendrocyte differentiation and remyelination

Previous studies have reported that microglia contribute to OLs differentiation and myelination by adopting a pro-regenerative phenotype and secreting growth factors (Hagemeyer et al., 2017; Miron et al., 2013). Thus, to examine whether miRNA expression loss in microglia has any effect on OLs differentiation, OPCs were co-cultured with endogenous *Dicer1*-inhibited primary microglia using siRNAs (Fig. 3A and B). After three days of differentiation, we found significantly fewer MBP+ cells in the presence of miRNA-deficient microglia (Fig. 3C and D, siControl 4.4 ± 0.33 % vs siDicer1 3.3 ± 0.13 % of nucleated cells) suggesting the requirement of microglial *Dicer1* to complete the OLs differentiation process.

Further, to examine the importance of microglia-specific miRNA expression during remyelination, we injected tamoxifen (TMX) to Cx3cr1^{creERT2}/Dicer1$^{fl/fl}$ and Tmem119^{creERT2}/Dicer1$^{fl/fl}$ male animals to induce *Dicer1* deletion in microglia/macrophage population, followed by cuprizone-induced demyelination for 6 weeks, followed by 6 weeks on regular diet for remyelination (Fig. 3E and R). At the end of the remyelination period, brain tissue was collected from both mouse models and processed for immunohistochemical analysis. We started by analyzing the effect of *Dicer1* loss on the microglia population during remyelination and observed a minor decrease in IBA1-positive cells in Cx3cr1^{creERT2} Cre + animals compared to the control (Cre−) group (Fig. 3H vs 3I, and 3O). Immunostaining of serial brain sections for PLP (Fig. 3F vs 3G) showed 21 % less myelin-occupied areas in CC of Cre + mutant than Cre− control animals (Fig. 3N). To understand whether decreased PLP staining (remyelination delay/failure) in Cre + mutant animals was related to differences in the numbers of mature OLs, we immunostained serial brain sections with anti-APC antibody and found no significant differences in APC+/OLIG2+ cell numbers between the two groups (Fig. 3J vs 3 K, and 3P). On the contrary, we observed ~41 % increase of PDGFRα+/OLIG2+ OPCs in Cre + mutant animals compared to the control group (Fig. 3L vs 3 M, and 3Q). Furthermore, in the Tmem119^{creERT2}/Dicer1$^{fl/fl}$ model, where *Dicer1* deletion is restricted to CNS resident microglia, Cre +

mice also exhibited a 30 % reduction in the PLP+ area (myelin content) compared to Cre− controls during remyelination (Fig. 3S vs 3 T, and 3a). Despite the reduction in myelin content, the density of IBA1+ microglia/macrophages were found to be similar between Cre + and Cre− mice (Fig. 3U, V and b), suggesting that the *Dicer1* loss does not alter overall numbers but might impair their function. Like the Cx3cr1^{creERT2} model, Tmem119^{creERT2} Cre + mice also displayed no significant change in the numbers of APC+/OLIG2+ mature oligodendrocytes (Fig. 3W, X, and c). Additionally, the number of PDGFRα+/OLIG2+ oligodendrocyte precursor cells were 60 % higher during remyelination in the context of CNS resident microglia-specific Dicer1 deletion (Cre− vs Cre+, Fig. 3Y vs 3Z, and 3d).

3.4. Microglial Dicer1 deletion amplifies inflammatory responses during demyelination and remyelination

To investigate the impact of *Dicer1* deletion during demyelination and remyelination, RNA-seq analysis was performed on FACS-sorted microglia (CD45^{int}CD11b+) from naïve Cx3cr1^{creERT2}/ Dicer1$^{fl/fl}$ male mice (Fig. 4A). As expected, Cre-recombinase-mediated *Dicer1* ablation led to a significant decrease in endogenous microglial/macrophages *Dicer1* expression (38 % of Cre− control mice, Fig. 4B). To further ensure microglia-specific transcriptome enrichment, we checked cell-specific gene expression from other CNS cell types and found that enriched genes were mainly contributed by microglia (Supplementary Figure S2A), thus confirming enriched microglial cell sorting. Comparative DEGs analysis between Cx3cr1^{creERT2} Cre− control and Cre + mutant animals revealed 594 upregulated and 554 downregulated genes (>1 log2Fold change and $p < 0.01$, Supplementary Figure S2B, Supplementary file 1). Moreover, Gene Ontology (GO) annotation of enriched biological processes ($p < 0.05$) showed altered genes to be associated with cell division/ cycle, and cholesterol homeostasis, among others (Supplementary Figure S2C and S2D).

While analyzing DEGs at the peak of demyelination (6 weeks of cuprizone treatment, Cup-6w) between Cre + *Dicer1* knockout and Cre− control animals, 355 genes were upregulated and 135 downregulated in the Cre + group (Fig. 4C, Supplementary file 2). However, after 6 weeks of remyelination (Cup-6w + 6), the number of differentially expressed genes (DEGs) were dramatically reduced (27 genes upregulated and 8 downregulated, Fig. 4D, Supplementary file 3), indicating that *Dicer1* loss has a more pronounced effect during demyelination than remyelination. To identify altered pathways associated with DEGs, Gene Set Enrichment Analysis (GSEA) was performed, which revealed significant upregulation of inflammatory and immune response pathways in *Dicer1*-deficient microglia, particularly during demyelination. These included the *IL-2/ IL-6/JAK/STAT* and interferon signaling pathways, along with activation of the complement system (Fig. 4E, Supplementary file 4). Notably, during remyelination, some inflammatory pathways including those related to *Wnt/β-catenin*, *KRAS* signaling, and oxidative stress (Fig. 4F, Supplementary file 4) remained dysregulated. Closer examination of specific inflammatory genes showed marked upregulation of pro-inflammatory markers such as *Ifng, Il1a, and Cxcl10* in Cre + animals during demyelination (Fig. 4G), while expression of genes like *Cxcl9, Osm, Irg1,* and *Nfkbia* remained elevated even during the remyelination phase (Fig. 4H), suggesting a persistent inflammatory phenotype in *Dicer1*-deficient microglia.

Additionally, to validate the transcriptomic findings at the protein level, we used a cytokine array (Fig. 4I) panel and showed that several pro-inflammatory cytokines, including *ICAM-1, IFN-γ, IL-16, M-CSF,* and *CXCL12,* were significantly upregulated in Cx3cr1^{creERT2} Cre + mice brain lysate during demyelination (Fig. 4J and K). Notably, these cytokines remained elevated in Cre + mutant mice brain during remyelination (Fig. 4L and M), reinforcing the observation that *Dicer1* deficiency sustains an inflammatory response beyond the demyelination phase.

Further supporting these findings, examination of TMEM119 expression, a CNS resident homeostatic microglia-specific marker, revealed that *Dicer1* deletion influenced microglial activation during demyelination (Supplementary Figure S3). In the Cx3cr1^{creERT2} line, TMEM119 expression was significantly elevated in Cre + compared to Cre− control animals during demyelination (Supplementary Figure S3O vs S3P, and S3S). This increase in TMEM119 was accompanied by elevated IBA1 expression (Supplementary Figure S3I vs S3J), suggesting both resident microglia and microglia/macrophage activation in *Dicer1*-deficient conditions during demyelination. In contrast, in the Tmem119^{creERT2} model, Cre + compared to Cre− group exhibited a decrease in TMEM119 expression during demyelination (Supplementary Figure S3h vs S3i, and S3l), indicating potential differences in resident microglial regulation by the loss of *Dicer1* in Cx3cr1 and Tmem119 cells population, specifically during demyelination. However following remyelination, TMEM119 expression in the Cx3cr1^{creERT2} model showed a decline trend (Supplementary Figure S3S). TMEM119 levels in the Tmem119^{creERT2} mouse model following remyelination was however significantly higher possibly suggesting restoration of microglial homeostasis. This dichotomy of resident microglial expression patterns following loss of *Dicer1* during demyelination and remyelination requires further investigation.

3.5. Dicer1 deletion in microglia enhances microgliosis and dysregulates cell cycle pathways during the demyelination

To assess dysregulated biological pathways due to *Dicer1* deletion in microglia/macrophages during demyelination, we performed GO (Gene Ontology) analysis of DEGs in Cx3cr1^{creERT2}/Dicer$^{fl/fl}$ mice. GO analysis revealed significant enrichment in biological processes related to the cell cycle, mitotic nuclear division, and chromosome segregation, among others (Fig. 5A, Supplementary File 5). Heatmap analysis showed that several key genes involved in cell cycle regulation, including Ube2c, Bub1, Cdc20, and Kif4, were upregulated in Cre + microglia during demyelination (Fig. 5B). These findings suggest that *Dicer1* deletion disrupts cell cycle regulation and promotes a proliferative response in microglia during demyelination.

We then examined the effects of *Dicer1* deletion on microglial proliferation and activation during demyelination (Fig. 5C). BrdU incorporation and immunostaining for the microglial marker IBA1 revealed a significant increase (>4 folds) in the number of IBA1 + BrdU+ proliferating microglia in Cx3cr1 Cre + mice compared to Cre− controls (Fig. 5D vs 5E, and 5F), indicating that *Dicer1* deletion enhances microgliosis during demyelination, which could exacerbate the inflammatory response and contribute to disease progression in demyelinating conditions.

As PDGFRα+/OLIG2+ OPCs number was found to be higher during demyelination (Fig. 2), we also performed immunostaining for PDGFRα, OLIG2 and BrdU. Interestingly, no significant differences were observed in the number of PDGFRα+ BrdU+ proliferating OPCs (Fig. 5G vs 5 K, and 5O) or in the density of OLIG2+ oligodendrocytes (Fig. 5H vs 5 L, and 5P) between Cx3cr1^{creERT2} Cre− and Cre + mice. These results suggest that *Dicer1* deletion in microglia does not affect OPCs proliferation or oligodendrocyte population during demyelination. However, feeding CUP to mice triggers apoptosis in mature OLs while leaving the population of OPCs unaffected, and does not alter the formation of new OLs during CUP-mediated WM (CC) demyelination (Chapman et al., 2023; Vega-Riquer et al., 2019). Thus, analyzing markers for mature OLs and apoptosis, a marked increase (~9 fold) in the number of APC+ and cleaved caspase 3 (CC3+) (APC+/CC3+) apoptotic oligodendrocytes was observed in Cx3cr1 Cre + mice compared to Cre− controls (Fig. 5Q–5V, and 5W), indicating that *Dicer1* deletion promotes mature OLs apoptosis during demyelination.

3.6. Dicer1 deficiency impairs microglial phagocytosis during demyelination and Remyelination, leading to impaired myelin clearance

Cuprizone induced demyelination significantly activate microglia and transform them into a phagocytic phenotype to actively remove myelin debris. Thus, to examine the impact of *Dicer1* deletion on microglial phagocytosis during demyelination and remyelination, we assessed myelin clearance and microglial activity in Cx3cr1^{creERT2} Cre + and Cre− mice. Immunohistochemical analysis of the CC during demyelination (Fig. 6A and B) and remyelination (Fig. 6C and D) revealed that Cre + mice exhibited significantly higher levels of degraded myelin protein (dMBP+) within IBA1+ microglia compared to Cre− controls. Quantification of dMBP+ staining in IBA1+ microglia (Fig. 6E) confirmed a significant increase in degraded MBP in Cre + mice during both demyelination and remyelination, highlighting that microglia in Cre + mice were overwhelmed with accumulated debris. Moreover, CD68, a marker of active phagocytosis, was significantly elevated in Cre + microglia compared to Cre− mice during both demyelination and remyelination (green pseudo colour, Fig. 6A–6D, and 6F). However, CD68 expression was reduced in Cre + mice during remyelination relative to demyelination, suggesting that although Cre + microglia remain phagocytically active, their efficiency decreases over time as they become overwhelmed by the high myelin debris load. Further to support degraded myelin presence during remyelination in Cre + animals, Oil Red O staining which marks lipid accumulation from degraded myelin, was performed in serial sections from demyelination/remyelination cohorts. Histochemical examination revealed increased lipid deposition in CC region of Cre + animals during both demyelination and remyelination compared to Cre− controls (Fig. 6G–6K), indicating that phagocytosed myelin debris was not adequately cleared, leading to lipid buildup within the microglia. This lipid accumulation further suggests that *Dicer1*-deficient microglia cannot degrade the engulfed myelin effectively. To further support above in vivo findings, we performed an in vitro phagocytosis assays using *Dicer1* knockout (KO) BV2 microglial cells. After introducing purified mouse brain myelin to the cultures, western blot analysis showed increased levels of MBP in *Dicer1* KO cells compared to controls, reflecting impaired degradation of phagocytosed myelin (Fig. 6L and M). This result further suggests that the absence of *Dicer1* impairs the microglia's ability to process

myelin debris efficiently, leading to its accumulation. Interestingly, Gene Set Enrichment Analysis (GSEA) of the RNA sequencing dataset also revealed significant downregulation of the phagocytosis pathway in Cx3cr1 Cre + microglia during both demyelination (NES = −1.16, FDR = 0.047) and remyelination (NES = −1.69, FDR = 0.0001) (Fig. 6N and O). Heatmaps of phagocytosis-related genes showed reduced expression of key genes involved in microglial phagocytosis, such as *C3, Thbs1, Rab34, Stap1, Sirpb1a, Rara, Sirpb1b, Treml4* and *Sirpb1c*, during both demyelination and remyelination (Fig. 6P and Q). These findings indicate that although Cre + microglia phagocytose more debris, their ability to continue efficient phagocytic activity declines due to an impaired capacity for myelin degradation.

4. Discussion

Various studies have reported cell intrinsic/extrinsic effects of *Dicer1*-regulated miRNAs on target gene regulation in the contexts of both normal cell function and disease conditions, including a recent finding suggesting that miRNA-targeted gene regulation contributes to intercellular cell signaling and thus affects proper functioning and development of target cells (Tao et al., 2011). In this study, the initial screening of MS brain white matter demyelinating lesions showed decreased Dicer protein expressing cells in the lesion core (LC), particularly of the IBA1+ microglia/macrophages cell population. Combining with CUP fed mouse model of MS disease, here we demonstrated the importance of microglial miRNA expression in demyelinating/remyelinating conditions using two independent TMX inducible *Dicer1*-ablated microglial (Cx3cr1^{creERT2} and Tmem119^{creERT2}) mouse lines. *Dicer1*-ablated adult microglia did not affect either brain myelin content or cause changes in OPC/OL populations, despite the reduction in IBA1+ cells in both genotypes maintained on a normal diet. However, CUP-induced extensive demyelination led to hyperactive and proliferative microglia with impaired myelin processing and lipid accumulation in Cre + mutant animals. This impairment highlights the necessity of *Dicer1*-dependent miRNA regulation for optimal microglial function during demyelination. Furthermore, *Dicer1*-deficient microglia exhibit a persistent inflammatory environment, characterized by elevated expression of pro-inflammatory cytokines, and impaired phagocytic activity which persisted during the remyelination phase. These observations demonstrate that while microglia are activated in response to myelin damage, *Dicer1* deficiency disrupts their ability to resolve inflammation, impairing the transition to a reparative state.

Dicer1, a terminal endonuclease, is indispensable for the biogenesis of mature miRNAs and is associated with post-transcriptional regulation of the target gene. *Dicer1*-dependent miRNAs have been reported to play roles in various aspects of cell development like cell cycle progression, cell division, cell maturation, and survival processes, including neurons, glia, and immune cells (Kuipers et al., 2010; Liu et al., 2017; Suárez et al., 2008). The observed reduction in microglial cell numbers in *Dicer1*-ablated mice could be attributed to miRNA-dependent mechanisms for DNA repair and genome integrity (Fischer et al., 2015; Swahari et al., 2016; Varol et al., 2017). Interestingly, RNA-seq data revealed dysregulated expression of genes related to cell cycle/division/DNA damage checkpoint regulation functions (*Ccne1, Ccne2, E2f1, E2f7, E2f8, Myc, Aurka, Ccnb1, Ccnb2, Cdc25c,*

Pkmyt1, Plk1) (Fischer et al., 2015; Shen et al., 2020), aligning with prior reports linking *Dicer1* loss to impaired microglial survival (Varol et al., 2017).

To understand microglia miRNAs role, we applied two animal models to evaluate the effects of *Dicer1* loss during demyelination/remyelination phases: 1) Cx3cr1-positive microglia/macrophages, and 2) Tmem119, specific to the CNS-confined microglia population. Both *Dicer1*-ablated mouse lines showed similar IBA1+ microglia population decline in the CC (WM region) along with hyperactive phenotype at the peak of demyelination (6 weeks of CUP feeding). However, the extent of demyelination appeared to be lesser in the Tmem119^{CreERT2} line compared to Cx3cr1^{CreERT2}, which might be associated with peripheral involvement of Cx3cr1-positive cells during demyelination (Kaddatz et al., 2021). We also noticed varied expression of microglia markers, IBA1 and TMEM119, between Cx3cr1^{creERT2} and Tmeme119^{creERT2} mouse lines which might be associated with varied transgene recombination efficacy (Faust et al., 2023). A further validation using another microglia homeostatic markers like P2RY12, GPR56, SERPINE2, is warranted (Zrzavy et al., 2017). A recent report of a single-cell RNAseq study from CUP-mediated mice suggests impairment of genes related to disruption of the blood-brain barrier (BBB) and tight junction proteins (Zia et al., 2022). We checked the demyelination RNA-seq gene dataset specific to border-associated macrophages (BAM) and found significant downregulation in gene expression at the peak of demyelination (*Lyz2, Cybb, Mrc1, Ifitm2/3*) (Pettas et al., 2022). As Cx3cr1 is expressed by BAMs, whereas Tmem119 is confined to the parenchymal microglia population (Dermitzakis et al., 2023), a detailed future study will be required to understand the differences between these two mouse lines specific to demyelination. One limitation of the present study might be sample selection during cell sorting stage, as we took whole brain microglia/macrophages sorting approach for bulk RNAseq analysis, rather than only affected CC (white matter) region. Future study using single cell RNAs sequencing approach from affected CC region of demyelinating/remyelinating cohorts has been planned to probe microglia specific factors. Moreover, we have also planned to evaluate transcriptional changes in CNS resident microglia *Dicer1* KO (Tmem119^{creERT2}) undergoing demyelination/remyelination paradigm similar to Cx3cr1 cohort, presented in this study.

Clearance of myelin debris, followed by recruitment and proliferation of OPCs and differentiation into mature myelinating OLs, are critical steps for successful remyelination in demyelinating diseases like MS (Poliani et al., 2015). Despite extensive demyelination after 6 weeks of CUP feeding, we noticed increased OPCs number during demyelinating and remyelinating stages in *Dicer1* KO animals. As the presence of degraded myelin impairs the recruitment and differentiation of OPCs (Neumann et al., 2009), excessive leftover degraded myelin and reduced phagocytosis-related genes during demyelination and remyelination might be responsible for arresting OPCs at the precursor stage, leading to remyelination delay/failure in *Dicer1* KO animals. During demyelination, *Dicer1*-deficient microglia exhibited significant upregulation of pro-inflammatory pathways, including *IL-2/IL-6/JAK/STAT* and interferon signaling pathways, along with elevated cytokine levels (*IFN-γ, IL-16, M-CSF*). Interestingly, cytokine array data revealed persistent upregulation of *IFN-γ, IL-16, M-CSF*, and adhesion molecules such as *ICAM-1* and *CXCL-12*, which are involved in immune recruitment, microglial activation, and phagocytic activity. Wnt/β-

catenin signaling pathway is pivotal for microglial activation (Halleskog et al., 2011; Halleskog and Schulte, 2013), during remyelination, this pathway is notably upregulated in *Dicer1* deficient microglia, highlighting their prolonged immune-activated state. Hence, this inability to resolve inflammation may interfere with OPC differentiation, further delaying remyelination. This finding aligns with reports that prolonged inflammatory signaling disrupts the reparative capacity of CNS-resident microglia (Jin and Yamashita, 2016; Miron et al., 2013).

Oligodendrocyte loss is a key pathological feature in demyelinating diseases such as MS, and increased apoptosis of OL cell population may impair remyelination and recovery process. The combination of enhanced microgliosis and elevated OLs apoptosis in *Dicer1*-deficient microglia suggests that the absence of *Dicer1* disrupts the protective role of microglia in maintaining tissue homeostasis during demyelination (Miron et al., 2013). By promoting microglial hyperactivation and mature OLs loss, *Dicer1* deficiency may contribute to exacerbate neuroinflammation and demyelination, leading to worsened disease outcomes. Furthermore, co-culture experiment demonstrated that *Dicer1*-deficient microglia failed to support OPC differentiation into mature OLs, highlighting *Dicer1*'s critical role in microglia-mediated paracrine signaling. The microglial role in remyelination extends beyond debris clearance to include paracrine signaling through cytokines such as IFN-γ, IL-16, and M-CSF. Among the identified cytokines, IFN-γ directly influences oligodendrocyte apoptosis (Vartanian et al., 1995), IL-16 enhances immune cell recruitment during inflammation (Hridi et al., 2021) whereas M-CSF, may hinder myelin repair under chronic expression (Hagan et al., 2020) and their presence during *Dicer1*-deficient conditions likely affects OPC maturation. Future investigations using single-cell RNA sequencing of lesion areas, such as the corpus callosum, will be vital to discern the balance between pro-reparative and inflammatory effects of these cytokines, potentially identifying novel therapeutic targets to enhance remyelination.

In demyelinating diseases like MS, degraded myelin accumulates in the lesion area, and phagocytic cells like microglia and infiltrating macrophages clear myelin debris, which is a prerequisite for a successful repair process (Kotter et al., 2006; Plemel et al., 2013; Shen et al., 2021). *Dicer1*-ablated microglia exhibited impaired myelin phagocytosis and processing, leading to heightened myelin loss at the peak of demyelination and a significant delay in myelin clearance during both demyelination and remyelination phases. Interestingly, RNA-seq analysis of FACS sorted microglia during demyelination and remyelination showed significant downregulation in phagocytosis-related genes (*Rab34 Thbs1, Stap1, Sirpb1a, C3, Sirpb1b, Rara, Sirpb1c, Treml4*) (Elberg et al., 2019; Grajchen et al., 2020) in *Dicer1*-deficient microglia, corroborating their reduced functional capacity. The deficiency of *Dicer1* in CNS microglia and macrophages significantly hampers the efficient clearance of myelin debris, a process reliant on lysosomal degradation of internalized myelin debris. This dysfunction is a contributing factor to the delayed remyelination observed in *Dicer1* knockout models, underscoring the crucial relationship between myelin debris clearance and the mechanisms underlying demyelination and neurodegeneration (Kotter et al., 2006; Lampron et al., 2015b; Plemel et al., 2013) Moreover, cholesterol homeostasis genes (*Ldlr, Sqle, Fabp5*) were also significantly downregulated in *Dicer1*-deficient microglia, even in the absence of overt activation. As cholesterol metabolism is essential for membrane

integrity, signaling, and phagocytosis, its disruption may impair microglial function and predispose them to inflammation, as reported in neurodegenerative diseases (Aung and Balashov, 2015; Loving and Bruce, 2020; Nugent et al., 2020). These findings highlight the key role of *Dicer1* and its miRNAs in maintaining microglial homeostasis under steady-state conditions.

In conclusion, this study highlights the unique role of *Dicer1*-regulated miRNAs in maintaining microglial function during demyelination and remyelination. Loss of *Dicer 1* in microglial cells regulate myelin clearance, oligodendrocytes maturation/differentiation, and remyelination. Persistent inflammation and dysregulated cytokine expression underlies this remyelination deficit. Future investigations using single-cell and region-specific approaches will provide deeper insights into microglial regulation of CNS repair mechanisms.

Supplementary Material

Refer to Web version on PubMed Central for supplementary material.

Acknowledgments

The authors would kindly like to acknowledge Drs. Mihyun Hwang, Jenifer Powers, and Cornelia Bergman for their kind support in microglia FACS assay. The authors would like to acknowledge editorial support from Dr. Christopher Nelson. This work was supported by NINDS R01 NS123532 and NINDS R21 NS123546 to RD.

Data availability

Data will be made available on request.

Abbreviations:

APC	Adenomatous polyposis coli
ASPA	Aspartoacylase
CC	corpus callosum
CD68	Cluster of Differentiation 68
CNS	central nervous system
CC3	cleaved caspase 3
CUP	cuprizone
DAB	diaminobenzidine
DEGs	differentially expressed genes
DMEM	Dulbecco’s modified Eagle’s medium
FACS	fluorescence-activated single cell sorting
FBS	fetal bovine serum

GFAP	glial fibrillary acidic protein
GO	Gene Ontology
GSEA	Gene Set Enrichment Analysis
LC	lesion center
MBP	myelin basic protein
MHCII	major histocompatibility complex class II
miRNAs	microRNAs
MS	multiple sclerosis
NAWM	normal appearing white matter
NGS	normal goat serum
OLs	oligodendrocytes
OPCs	oligodendrocyte progenitor cells
ORO	Oil Red O
PDGFRα	platelet-derived growth factor receptor alpha
PFA	paraformaldehyde
PLP	Proteolipid Protein
TBST	tris-buffered saline with Tween-20
TMX	Tamoxifen
WML	white matter lesion

References

Aung LL, Balashov KE, 2015. Decreased Dicer expression is linked to increased expression of co-stimulatory molecule CD80 on B cells in multiple sclerosis. Mult. Scler 21, 1131–1138. [PubMed: 25480859]

Chapman TW, et al. 2023. Oligodendrocyte death initiates synchronous remyelination to restore cortical myelin patterns in mice. Nat. Neurosci 26, 555–569. [PubMed: 36928635]

Cignarella F, et al. 2020. TREM2 activation on microglia promotes myelin debris clearance and remyelination in a model of multiple sclerosis. Acta Neuropathol 140, 513–534. [PubMed: 32772264]

Dermitzakis I, et al. 2023. CNS border-associated macrophages: ontogeny and potential implication in disease. Curr. Issues Mol. Biol 45, 4285–4300. [PubMed: 37232741]

Djannatian M, et al. 2023. Myelination generates aberrant ultrastructure that is resolved by microglia. J. Cell Biol 222.

Dugas JC, et al. 2010. Dicer1 and miR-219 are required for normal oligodendrocyte differentiation and myelination. Neuron 65, 597–611. [PubMed: 20223197]

Dutta R, et al. 2019. Comprehensive autopsy program for individuals with multiple sclerosis. J. Vis. Exp 149, e59511. 10.3791/59511.

Elberg G, et al. 2019. Deletion of SIRPα (signal regulatory protein-α) promotes phagocytic clearance of myelin debris in Wallerian degeneration, axon regeneration, and recovery from nerve injury. J. Neuroinflammation 16, 277. [PubMed: 31883525]

Faust TE, et al. 2023. A comparative analysis of microglial inducible Cre lines. Cell Rep 42, 113031. [PubMed: 37635351]

Fischer M, et al. 2015. Indirect p53-dependent transcriptional repression of Survivin, CDC25C, and PLK1 genes requires the cyclin-dependent kinase inhibitor p21/CDKN1A and CDE/CHR promoter sites binding the DREAM complex. Oncotarget 6, 41402–41417. [PubMed: 26595675]

Grajchen E, et al. 2020. CD36-mediated uptake of myelin debris by macrophages and microglia reduces neuroinflammation. J. Neuroinflammation 17, 224. [PubMed: 32718316]

Hagan N, et al. 2020. CSF1R signaling is a regulator of pathogenesis in progressive MS. Cell Death Dis 11, 904. [PubMed: 33097690]

Hagemeyer N, et al. 2017. Microglia contribute to normal myelinogenesis and to oligodendrocyte progenitor maintenance during adulthood. Acta Neuropathol 134, 441–458. [PubMed: 28685323]

Halleskog C, Schulte G, 2013. Pertussis toxin-sensitive heterotrimeric G(alphai/o) proteins mediate WNT/beta-catenin and WNT/ERK1/2 signaling in mouse primary microglia stimulated with purified WNT-3A. Cell. Signal. 25, 822–828. [PubMed: 23266471]

Halleskog C, et al. 2011. WNT signaling in activated microglia is proinflammatory. Glia 59, 119–131. [PubMed: 20967887]

Hridi SU, et al. 2021. Increased levels of IL-16 in the central nervous system during Neuroinflammation are associated with infiltrating immune cells and resident glial cells. Biology (Basel). 10.

Hwang JY, et al. 2017. The emerging field of epigenetics in neurodegeneration and neuroprotection. Nat. Rev. Neurosci 18, 347–361. [PubMed: 28515491]

Jin X, Yamashita T, 2016. Microglia in central nervous system repair after injury. J. Biochem 159, 491–496. [PubMed: 26861995]

Kaddatz H, et al. 2021. Cuprizone-induced demyelination triggers a CD8-pronounced T cell recruitment. Glia 69, 925–942. [PubMed: 33245604]

Kotter MR, et al. 2006. Myelin impairs CNS remyelination by inhibiting oligodendrocyte precursor cell differentiation. J. Neurosci 26, 328–332. [PubMed: 16399703]

Kuhlmann T, et al. 2017. An updated histological classification system for multiple sclerosis lesions. Acta Neuropathol 133, 13–24. [PubMed: 27988845]

Kuipers H, et al. 2010. Dicer-dependent microRNAs control maturation, function, and maintenance of Langerhans cells in vivo. J. Immunol 185, 400–409. [PubMed: 20530258]

Lampron A, et al. 2015a. Inefficient clearance of myelin debris by microglia impairs remyelinating processes. J. Exp. Med 212, 481–495. [PubMed: 25779633]

Lampron A, et al. 2015b. Inefficient clearance of myelin debris by microglia impairs remyelinating processes. J. Exp. Med 212, 481–495. [PubMed: 25779633]

Liu S, et al. 2017. miR-219 attenuates demyelination in cuprizone-induced demyelinated mice by regulating monocarboxylate transporter 1. Eur. J. Neurosci 45, 249–259. [PubMed: 27873367]

Liu K, et al. 2021. Dicer deletion in astrocytes inhibits Oligodendroglial differentiation and myelination. Neurosci. Bull. 37, 1135–1146. [PubMed: 34106403]

Lloyd AF, et al. 2019. Central nervous system regeneration is driven by microglia necroptosis and repopulation. Nat. Neurosci 22, 1046–1052. [PubMed: 31182869]

Loving BA, Bruce KD, 2020. Lipid and lipoprotein metabolism in microglia. Front. Physiol 11, 393. [PubMed: 32411016]

Magner WJ, et al. 2016. Dicer and microRNA expression in multiple sclerosis and response to interferon therapy. J. Neuroimmunol 292, 68–78. [PubMed: 26943961]

Mehlem A, et al. 2013. Imaging of neutral lipids by oil red O for analyzing the metabolic status in health and disease. Nat. Protoc 8, 1149–1154. [PubMed: 23702831]

Mi G, et al. 2016. Cyclin-dependent kinase inhibitor flavopiridol promotes remyelination in a cuprizone induced demyelination model. Cell Cycle 15, 2780–2791. [PubMed: 27580304]

Miron VE, et al. 2013. M2 microglia and macrophages drive oligodendrocyte differentiation during CNS remyelination. Nat. Neurosci 16, 1211–1218. [PubMed: 23872599]

Nemes-Baran AD, et al. 2020. Fractalkine-dependent microglial pruning of viable oligodendrocyte progenitor cells regulates myelination. Cell Rep 32, 108047. [PubMed: 32814050]

Neumann H, et al. 2009. Debris clearance by microglia: an essential link between degeneration and regeneration. Brain 132, 288–295. [PubMed: 18567623]

Nugent AA, et al. 2020. TREM2 regulates microglial cholesterol metabolism upon chronic phagocytic challenge. Neuron 105 (837–854), e9.

Pettas S, et al. 2022. Profiling microglia through single-cell RNA sequencing over the course of development, aging, and disease. Cells 11.

Plemel JR, et al. 2013. Myelin inhibits oligodendroglial maturation and regulates oligodendrocytic transcription factor expression. Glia 61, 1471–1487. [PubMed: 23839973]

Plemel JR, et al. 2020. Microglia response following acute demyelination is heterogeneous and limits infiltrating macrophage dispersion. Sci. Adv 6, eaay6324. [PubMed: 31998844]

Poliani PL, et al. 2015. TREM2 sustains microglial expansion during aging and response to demyelination. J. Clin. Invest 125, 2161–2170. [PubMed: 25893602]

Sanjana NE, et al. 2014. Improved vectors and genome-wide libraries for CRISPR screening. Nat. Methods 11, 783–784. [PubMed: 25075903]

Schindelin J, et al. 2012. Fiji: an open-source platform for biological-image analysis. Nat. Methods 9, 676–682. [PubMed: 22743772]

Shen Y, et al. 2020. Targeting aurora kinase B alleviates spinal microgliosis and neuropathic pain in a rat model of peripheral nerve injury. J. Neurochem 152, 72–91. [PubMed: 31563141]

Shen K, et al. 2021. Multiple sclerosis risk gene Mertk is required for microglial activation and subsequent remyelination. Cell Rep 34, 108835. [PubMed: 33691116]

Shin D, et al. 2009. Dicer ablation in oligodendrocytes provokes neuronal impairment in mice. Ann. Neurol 66, 843–857. [PubMed: 20035504]

Suárez Y, et al. 2008. Dicer-dependent endothelial microRNAs are necessary for postnatal angiogenesis. Proc. Natl. Acad. Sci. USA 105, 14082–14087. [PubMed: 18779589]

Swahari V, et al. 2016. Essential function of Dicer in resolving DNA damage in the rapidly dividing cells of the developing and malignant cerebellum. Cell Rep 14, 216–224. [PubMed: 26748703]

Tao J, et al. 2011. Deletion of astroglial Dicer causes non-cell-autonomous neuronal dysfunction and degeneration. J. Neurosci 31, 8306–8319. [PubMed: 21632951]

Tripathi A, et al. 2019. Oligodendrocyte intrinsic miR-27a controls myelination and Remyelination. Cell Rep 29, 904–919.e9. [PubMed: 31644912]

Varol D, et al. 2017. Dicer deficiency differentially impacts microglia of the developing and adult brain. Immunity 46, 1030–1044.e8. [PubMed: 28636953]

Vartanian T, et al. 1995. Interferon-gamma-induced oligodendrocyte cell death: implications for the pathogenesis of multiple sclerosis. Mol. Med 1, 732–743. [PubMed: 8612196]

Vega-Riquer JM, et al. 2019. Five decades of Cuprizone, an updated model to replicate demyelinating diseases. Curr. Neuropharmacol 17, 129–141. [PubMed: 28714395]

Wlodarczyk A, et al. 2017. A novel microglial subset plays a key role in myelinogenesis in developing brain. EMBO J. 36, 3292–3308. [PubMed: 28963396]

Yip PK, et al. 2019. Docosahexaenoic acid reduces microglia phagocytic activity via miR-124 and induces neuroprotection in rodent models of spinal cord contusion injury. Hum. Mol. Genet 28, 2427–2448. [PubMed: 30972415]

Zhao X, et al. 2010. MicroRNA-mediated control of oligodendrocyte differentiation. Neuron 65, 612–626. [PubMed: 20223198]

Zia S, et al. 2022. Single-cell microglial transcriptomics during demyelination defines a microglial state required for lytic carcass clearance. Mol. Neurodegener 17, 82. [PubMed: 36514132]

Zrzavy T, et al. 2017. Loss of 'homeostatic' microglia and patterns of their activation in active multiple sclerosis. Brain 140, 1900–1913. [PubMed: 28541408]

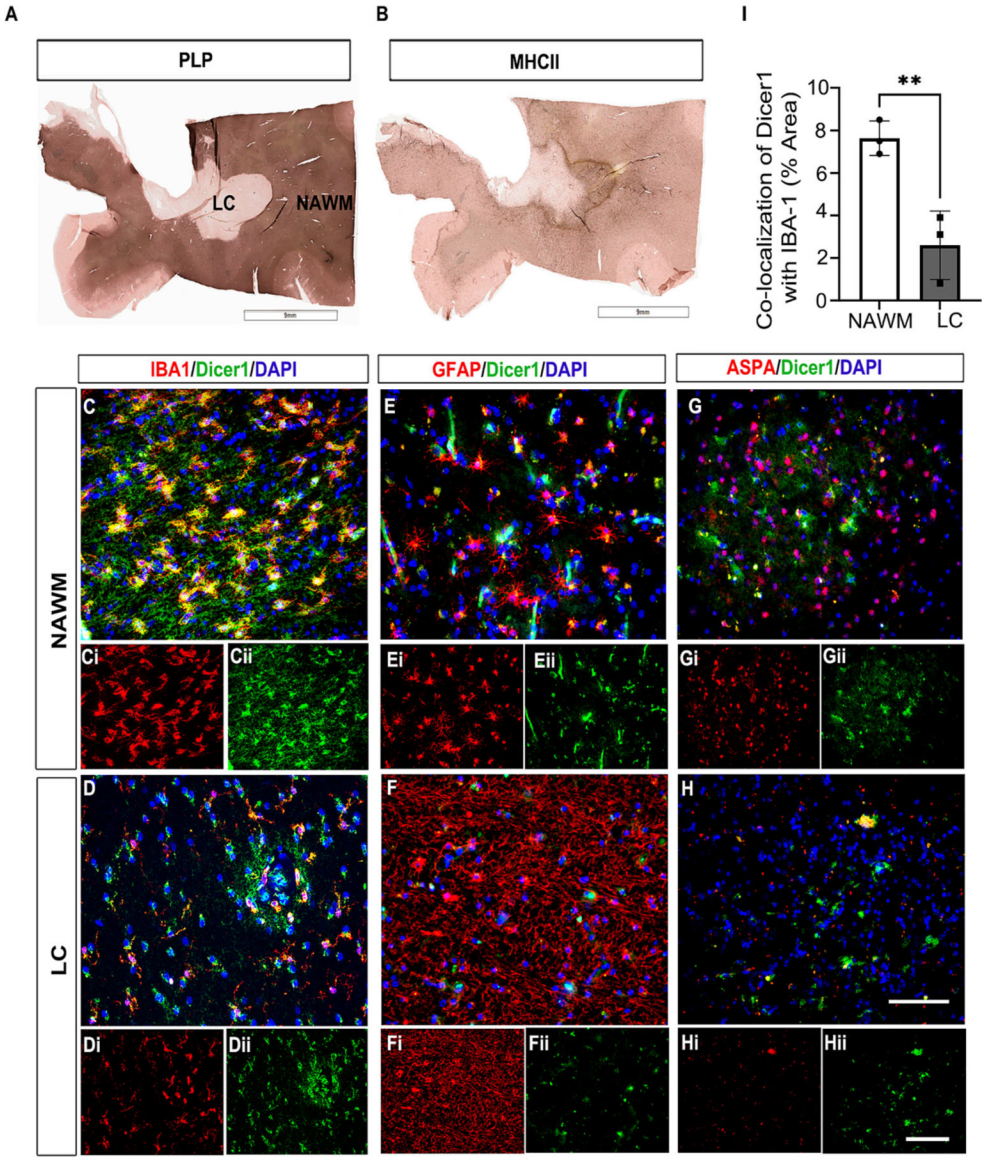

Fig. 1.

Dicer-Positive Microglia in MS Lesions.

(A-B) Representative DAB immunostained serial sections from a confirmed MS brain showing demyelinated lesion (PLP) and immune cell infiltration (MHCII). Scale bar – 9 mm. (C–H) Representative fluorescent labeled confocal images of serial MS brain sections showing Dicer (green) positive microglia/macrophages (IBA1, red), astrocytes (GFAP), and oligodendrocytes (ASPA) distribution across different regions of a MS lesion (WMLs) including normal-appearing white matter (NAWM), and lesion center (LC). Scale bar - 50 μm. (I) A bar graph illustrating the percentage of colocalization between IBA1 and *Dicer 1* staining in NAWM and LC. The error bar represents mean ± SEM, with a sample size of $n = 3$ MS patients. Statistical significance was determined by Student's t-test (two-sided) with $^{**}p < 0.01$. (For interpretation of the references to colour in this figure legend, the reader is referred to the web version of this article.)

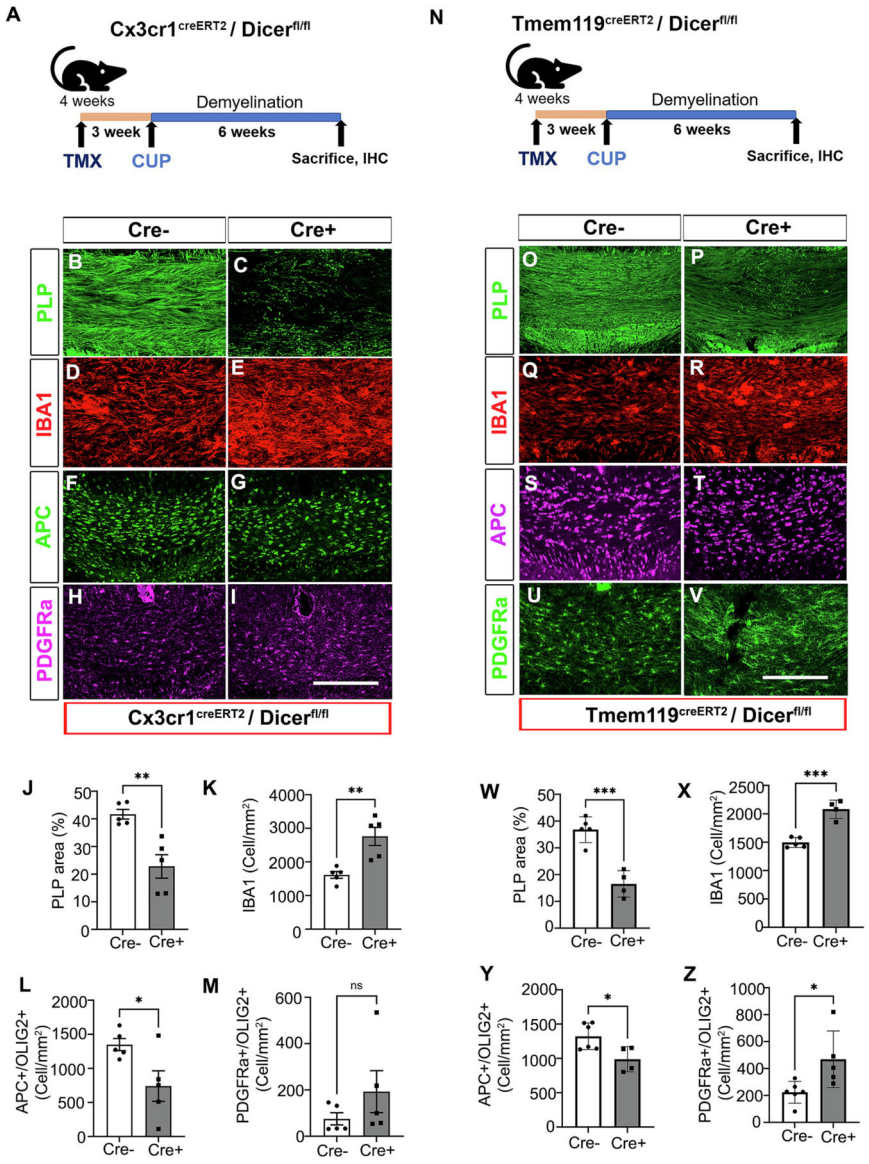

Fig. 2.

Dicer1 deleted microglial response to demyelination.

(A) Schematic illustration of Cx3Cr1^{creERT2}/Dicer$^{fl/fl}$ animals undergoing TMX treatment and CUP feeding. (B–I) Representative immunostained confocal images of myelin (PLP, B and C), microglia (IBA1, D and E), OLs (APC, F and G), and OPCs (PDGFRα, H and I) from TMX-injected Cx3cr1^{creERT2} Cre− control and Cre + mutant animals after six weeks of CUP feeding (n = 5). Scale bar - 50 μm. (J-M) Bar graphs showing myelin occupied area (J) and cell numbers (K, L, and M) in CUP-fed mouse brain CC. (N) Schematic illustration of Tmem119^{creERT2}/Dicer$^{fl/fl}$ animals undergoing TMX (tamoxifen) treatment and CUP (cuprizone) feeding. (O–V) Representative immunostained confocal images showing myelin (PLP, O and P), microglia (IBA1, Q and R), OLs (APC, S and T), and OPCs (PDGFRα, U and V) from TMX-injected Tmem119^{creERT2} Cre− control and Cre + mutant animals after six weeks of CUP feeding (n = 4–5). Scale bar = 50 μm. (W-Z) Bar graphs displaying the

quantification of myelin occupied area (W) and cell numbers (X, Y, and Z) in the corpus callosum (CC) of CUP-fed mouse brains. Error bars represent mean ± SEM. Statistical significance was determined by Student's *t*-test (two-sided) with *$p < 0.05$, **p < 0.01, ***$p < 0.001$ and ns indicating non-significance.

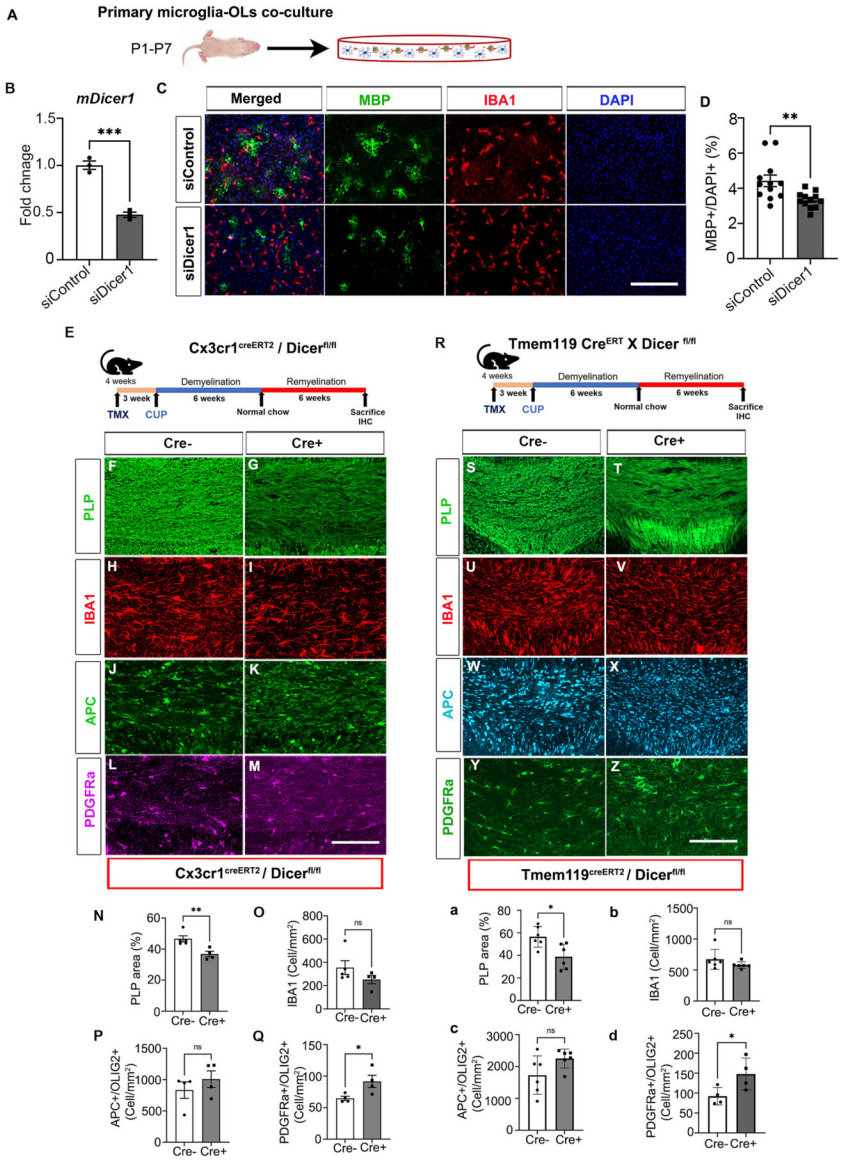

Fig. 3.

Microglial *Dicer1* affects Oligodendrocyte Differentiation and Efficient Remyelination. (A) Schematic illustration of siDicer1-treated P1 primary microglia co-cultured with P6–7 mouse primary OPCs. (B) qPCR analysis of *mDicer1* expression in microglia treated with siControl and siDICER1. GAPDH was used as an endogenous control for qPCR analysis ($n = 3$). (C) Representative immunofluorescence images (from three independent experiments with similar results) showing mouse primary OLs (MBP+ cells, green) and co-cultured with siDicer1-treated primary mouse microglia (IBA1+ cell, red). siControl- top row and siDicer1- bottom row. Nuclei were stained with DAPI (blue). Scale bar - 50 μm. (D) Quantitative analyses of MBP+ cells from OPCs/microglia co-cultures. Data represent mean ± SEM of MBP+ cell populations from 3 independent experiments. (E) Schematic illustration of Cx3cr1^{creERT2}/Dicer$^{fl/fl}$ animals undergoing TMX treatment, CUP feeding, and remyelination. (F-M) Representative immunostained confocal images of myelin (PLP,

F and G), microglia (IBA1, H and I), OLs (APC, J and K), and OPCs (PDGFRα, L and M) from TMX-injected Cx3cr1^{creERT2} Cre− control and Cre + mutant animals after six weeks of CUP feeding and then 6 weeks maintained on a normal diet (n = 4–5). Scale bar - 50 μm. (N-Q) Bar graphs showing myelin-occupied area (N) and cell numbers (O-Q) in remyelinated mouse brain CC. (R) Schematic illustration of TMEM119^{creERT2}/Dicer$^{fl/fl}$ mice undergoing tamoxifen (TMX) treatment followed by 6 weeks of cuprizone (CUP) feeding and subsequent 6-weeks on normal diet to study remyelination. (S-Z) Representative confocal images of remyelination in the corpus callosum (CC) showing myelin (PLP, S and T), microglia (IBA1, U and V), OLs (APC, W and X), and OPCs (PDGFRα, Y and Z) in TMX-injected Tmem119^{creERT2} Cre− control and Cre + mutant mice (n = 4–6). Scale bar: 50 μm. (a-d) Bar graphs displaying the remyelinated area (a) and cell counts for microglia, OLs, and OPCs (b-d) in the CC during remyelination. Error bars indicate mean ± SEM. Statistical significance was determined by Student's t-test (two-sided) with *p < 0.05, **p < 0.01, ***p < 0.001 and ns indicating non-significance. (For interpretation of the references to colour in this figure legend, the reader is referred to the web version of this article.)

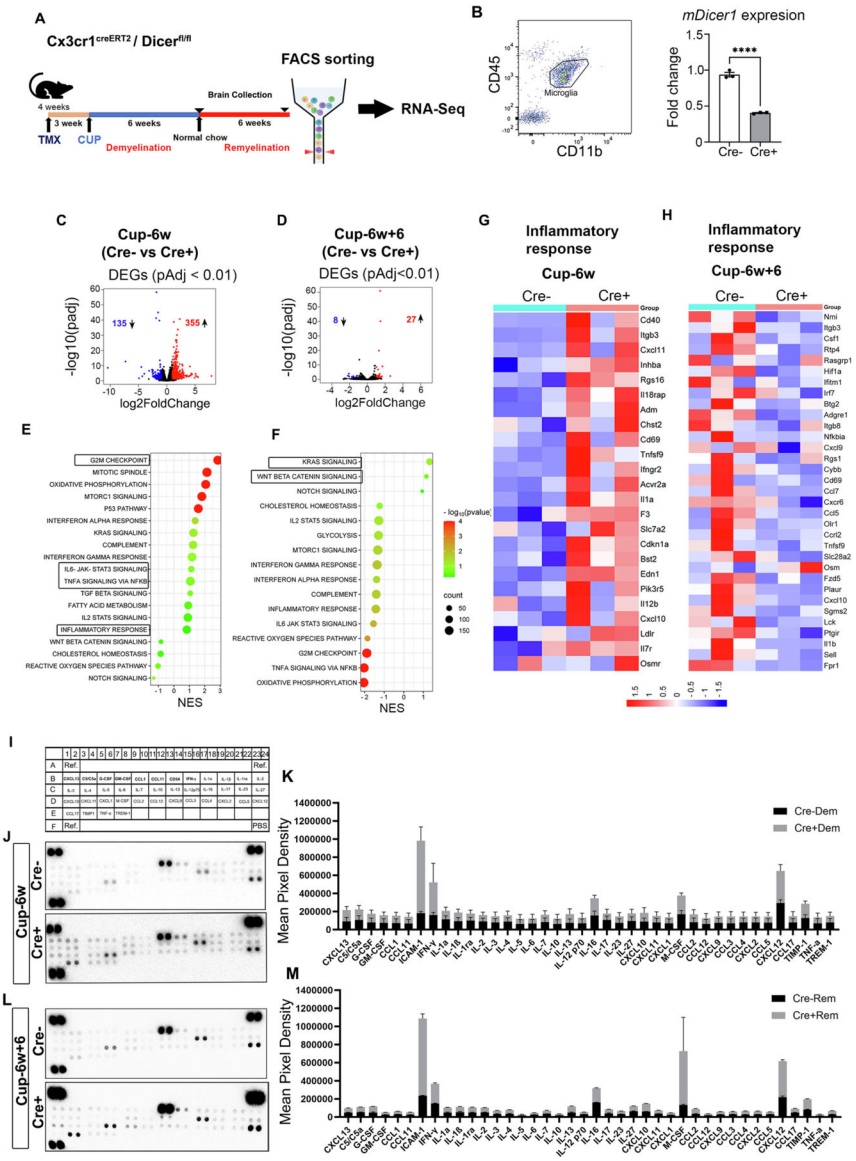

Fig. 4.

Impact of Microglial *Dicer1* Deletion on Inflammation during Demyelination and Remyelination.

(A) Experimental design showing tamoxifen (TMX) administration to induce Dicer1 deletion in Cx3cr1^{creERT2} microglia (Cre+), followed by cuprizone (CUP) diet for 6 weeks to induce demyelination, and then 6 weeks of remyelination on the normal chow. Microglia were isolated from Cx3cr1^{creERT2} (Cre− and Cre+) mouse brains using FACS sorting and analyzed by RNA sequencing. (B) Flow cytometric gating for microglial isolation, showing expression of CD11b and CD45 markers. The bar graph shows qPCR analysis of mDicer1 expression in FASC-sorted CD45^{int}/CD11b + microglia from naïve Cx3cr1^{creERT2} (Cre− and Cre+) animals (n = 3) treated with TMX only. GAPDH was used as an endogenous control for qPCR analysis. (C) Volcano plot showing differentially expressed genes (DEGs) (pAdj <0.01) between Cx3cr1^{creERT2} Cre− and Cre + microglia after 6 weeks of cuprizone-

induced demyelination (Cup-6w). (D) Volcano plot of DEGs ($p < 0.01$) in Cx3cr1^{creERT2} Cre− and Cre + microglia after 6 weeks of CUP diet followed by 6 weeks of remyelination (Cup-6w + 6). (E) Gene set enrichment analysis (GSEA) plot showing significant altered pathways in Cx3cr1^{creERT2} Cre− vs Cre + microglia at Cup-6w. (F) GSEA plot of significant pathways in Cx3cr1^{creERT2} Cre− vs Cre + microglia at Cup-6w + 6. (G) Heatmap showing expression of inflammatory response genes in Cx3cr1^{creERT2} Cre− and Cre + microglia at Cup-6w. (H) Heatmap of inflammatory response genes at Cup-6w/+6 in Cx3cr1^{creERT2} Cre− and Cre + microglia. (I) Layout of the cytokine protein array, showing the location of each cytokine on the membrane. (J, K) Protein array analysis of cytokine expression in Cx3cr1^{creERT2} (Cre− and Cre+) microglia at Cup-6w, visualized as dot blots (J) and quantified as mean pixel density (K). (L, M) Cytokine expression at Cup-6w + 6 was visualized as dot blots (L) and quantified as mean pixel density (M) during remyelination in Cx3cr1^{creERT2} Cre− and Cre + mice. Normalized Enrichment Score (NES). Error bars indicate mean ± SEM. Statistical significance was determined by Student’s t-test (two-sided) with ****$p < 0.0001$ and ns indicating non-significance.

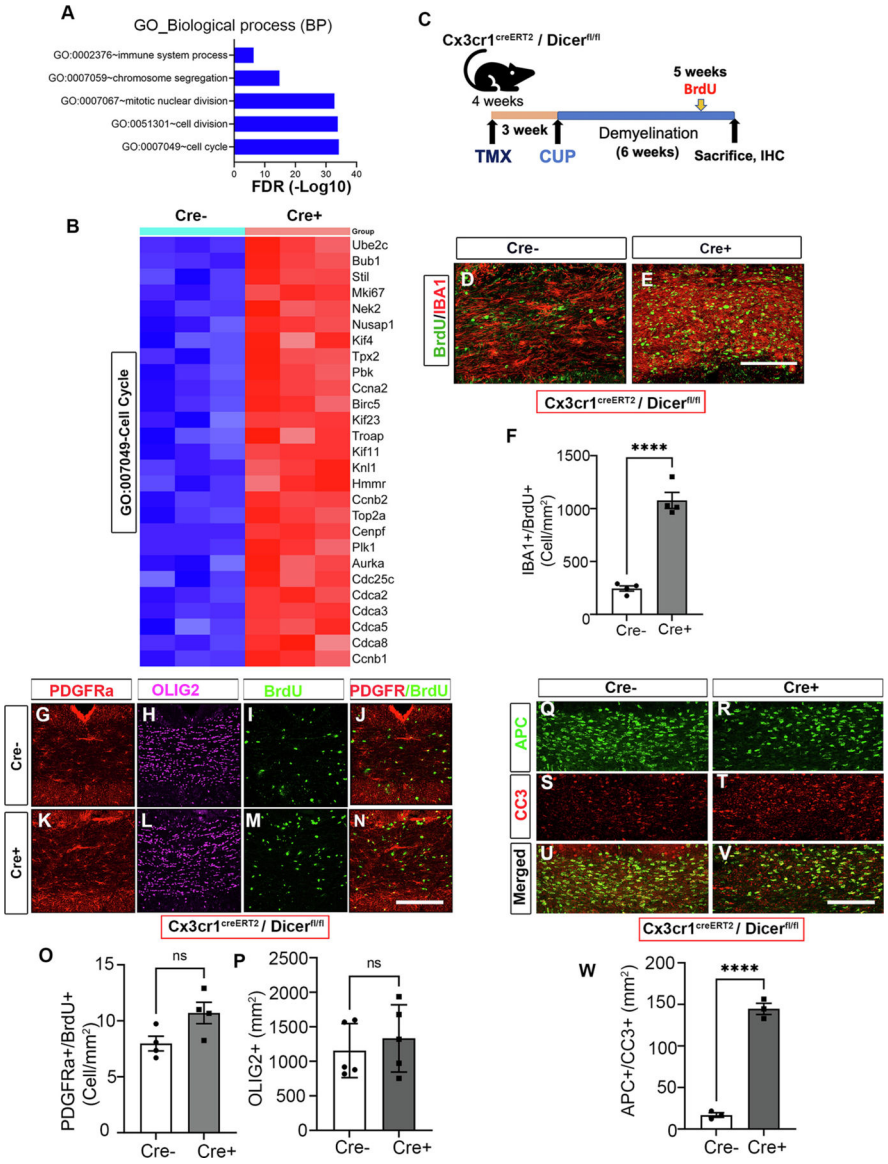

Fig. 5.

Dicer1 Deletion in Microglia Enhances Microgliosis and Dysregulates Cell Cycle Pathways During the Demyelination.

(A) Gene Ontology (GO) analysis of biological processes shows enrichment of cell cycle-related pathways in Cx3cr1^{creERT2} Dicer1-deleted microglia (Cre+) compared to controls (Cre−). (B) Heatmap illustrating dysregulated expression of key genes associated with the cell cycle in Cre + microglia during demyelination. Genes such as Mki67, Ccna2, and Plk1 are upregulated, indicating enhanced proliferation. (C) Schematic illustration of TMX treatment to induce Dicer1 deletion, followed by cuprizone (CUP) feeding and BrdU labeling to assess microglial proliferation. (D-E) Immunofluorescence images of BrdU (green) and IBA1 (red) staining in Cx3cr1^{creERT2} Cre − and Cre + mice during demyelination, indicating increased proliferation in Cre + microglia (n = 4). (F) Quantification of IBA1 + BrdU+ microglia reveals significant enhancement of microglial

proliferation in the Cx3cr1^{creERT2} Cre + group. (G-N) Immunostaining for PDGFRα (red), OLIG2 (magenta), and BrdU (green) shows no significant difference in OPCs proliferation between Cx3cr1^{creERT2} Cre − and Cre + groups (n = 4), shown as quantified bar graph in (O) and (P), respectively. (Q-V) Immunofluorescence staining of OLs (APC, green) and apoptotic marker (CC3, red) indicates increased apoptosis of mature OLs in the Cx3cr1^{creERT2} Cre + compared to Cre− group (n = 3). (W) Quantification of APC + CC3+ apoptotic oligodendrocytes shows a significant increase in the Cx3cr1^{creERT2} Cre + group. Error bars indicate mean ± SEM. Statistical significance was determined by Student's t-test (two-sided) with ****$p < 0.0001$ and ns indicating non-significance. (For interpretation of the references to colour in this figure legend, the reader is referred to the web version of this article.)

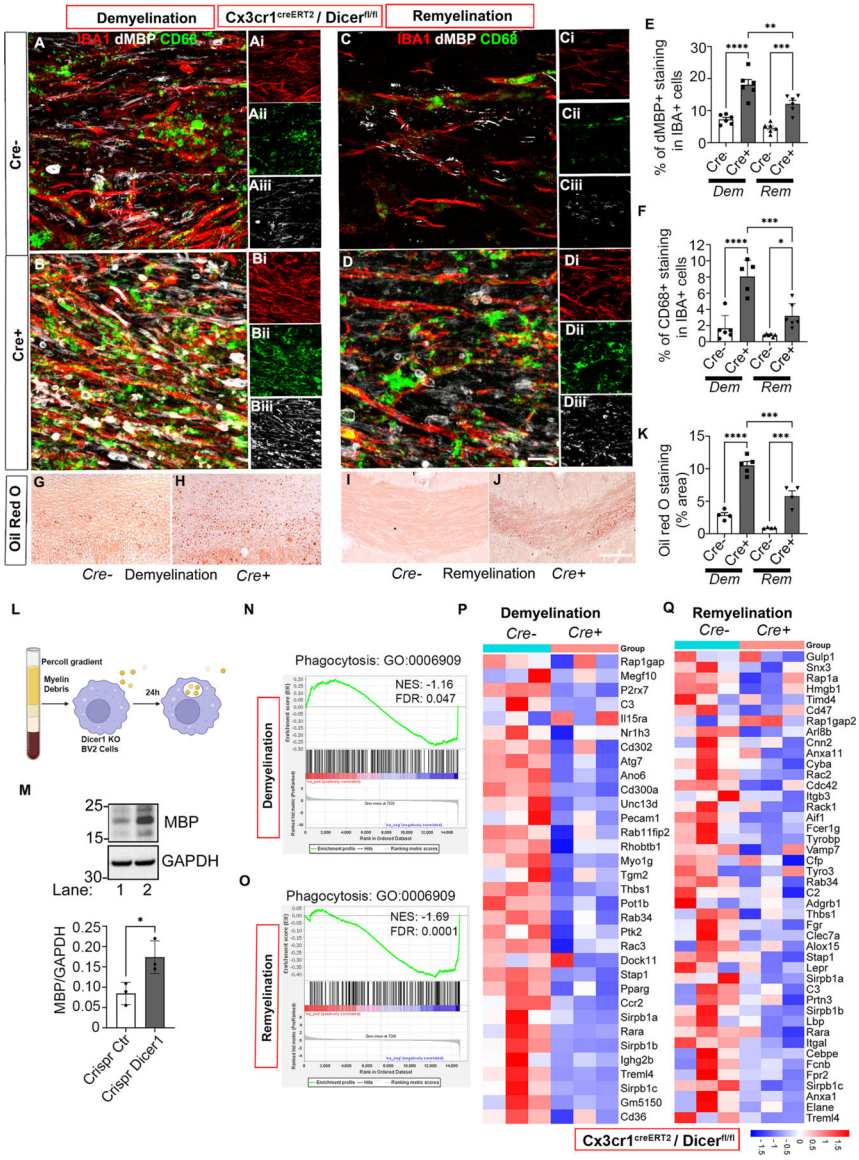

Fig. 6.

Dicer1 deficiency impairs microglial phagocytosis during demyelination and remyelination, leading to impaired myelin clearance.

(A-D) Immunohistochemical staining of brain sections during demyelination and remyelination. (A-B) Representative images of demyelination in Cx3cr1^{creERT2} control (Cre−) (A) and *Dicer1*-deficient (Cre+) (B) mice showing IBA1+ microglia (red), degraded myelin (dMBP, white), and CD68 (green). Insets (Ai-Aiii, Bi-Biii) showing IBA1, dMBP, and CD68 staining, respectively (n = 6). (C–D) Representative images during remyelination in Cx3cr1^{creERT2} Cre− (C) and Cre + (D) conditions. Insets (Ci-Ciii, Di-Diii) showing IBA1, dMBP, and CD68 staining (n = 5–6). (E) Quantification of the percentage of dMBP+ (degraded myelin basic protein) staining within IBA1+ cells show significantly higher myelin debris accumulation in Dicer1-deficient (Cre+) microglia compared to controls during both demyelination and remyelination. (F) Quantification of the percentage of

CD68+ staining within IBA1+ cells show increased phagocytic activation in *Dicer1*-deficient Cx3cr1^{creERT2} Cre + microglia during demyelination compared to Cre− controls. However, during remyelination, *Dicer1*-deficient microglia show a decrease in CD68+ expression compared to the demyelination phase. (G-J) Oil Red O staining for lipid accumulation in brain sections during demyelination (G-H) and remyelination (I-J) in Cx3cr1^{creERT2} Cre− (G, I) and Cre + (H, J) mice (n = 4–5). (K) Quantification of Oil Red O staining area shows increased lipid accumulation in *Dicer1*-deficient Cx3cr1^{creERT2} Cre + microglia compared to Cre− controls during demyelination/remyelination. (L) Schematic of myelin debris phagocytosis assay in *Dicer1*-deficient BV2 microglial cells, where BV2 cells treated with Percoll gradient-purified myelin debris for 24 h. (M) Western blot analysis of MBP protein in Dicer1-KO (Crispr Dicer1) BV2 cells compared to control (Crispr Ctr). Quantification shows significantly decreased myelin debris clearance capacity (higher MBP density) in Dicer1 BV2 knockout cells (n = 3). (N and O) Gene Set Enrichment Analysis (GSEA) showing significant downregulation of phagocytosis-related genes in Dicer1-deficient Cx3cr1^{creERT2} Cre + microglia during demyelination (P, NES: −1.16, FDR: 0.047) and remyelination (Q, NES: −1.69, FDR: 0.0001). (P and Q) Heatmaps showing the expression of phagocytosis-related genes in Cx3cr1^{creERT2} Cre−/Cre + during demyelination (P) and remyelination (Q). Red indicates upregulation, and blue indicates downregulation. Error bars indicate mean ± SEM. Statistical significance was determined by Student's t-test (two-sided, M)/one-way ANOVA with Tukey's test for multiple comparisons (E, F, and K) with *$p < 0.05$, **p < 0.01, ***$p < 0.001$, ****p < 0.0001 and ns indicating non-significance. (For interpretation of the references to colour in this figure legend, the reader is referred to the web version of this article.)